



# Compressive properties of 3-D printed Mg–NiTi interpenetrating-phase composite: Effects of strain rate and temperature

Mingyang Zhang<sup>a,b</sup>, Qin Yu<sup>c</sup>, Zengqian Liu<sup>a,b,\*</sup>, Jian Zhang<sup>a</sup>, Da Jiao<sup>a</sup>, Shujun Li<sup>a,b</sup>, Hui Peng<sup>d</sup>, Qiang Wang<sup>e,\*\*</sup>, Zhefeng Zhang<sup>a,b</sup>, Robert O. Ritchie<sup>f</sup>

<sup>a</sup> Shi-Changxu Innovation Center for Advanced Materials, Institute of Metal Research, Chinese Academy of Sciences, Shenyang, 110016, China

<sup>b</sup> School of Materials Science and Engineering, University of Science and Technology of China, Hefei, 230026, China

<sup>c</sup> Materials Sciences Division, Lawrence Berkeley National Laboratory, Berkeley, CA, 94720, USA

<sup>d</sup> National Key Laboratory of Shock Wave and Detonation Physics, Institute of Fluid Physics, Mianyang, 621900, China

<sup>e</sup> School and Hospital of Stomatology, China Medical University, Shenyang, 110001, China

<sup>f</sup> Department of Materials Science and Engineering, University of California Berkeley, Berkeley, CA, 94720, USA

## ARTICLE INFO

### Keywords:

Interpenetrating-phase composite  
Energy absorption  
Damage mechanisms  
3-D printing  
Magnesium  
Nitinol

## ABSTRACT

For composite materials applied for energy absorption and vibration/noise reduction, it is of particular significance to clarify the role of strain rate and temperature on their mechanical properties. Here we present a study on the effects of strain rate (from  $10^{-3} \text{ s}^{-1}$  to  $1 \text{ s}^{-1}$ ) and temperature (from room temperature to  $350 \text{ }^\circ\text{C}$ ) on the compressive properties of a 3-D printed Mg–NiTi interpenetrating-phase composite, which features high energy absorption efficiency and good damping capacity. Within the regimes of strain rate and temperature, the composite constantly exhibits a stable stress plateau on the stress-strain curves, yet displays markedly different damage mechanisms depending on the specific strain rate and temperature. The 3-D interpenetrating-phase architecture promotes an effective stress transfer in the composite and resists the propagation of local damages, thereby conferring a high strengthening efficiency and outstanding damage tolerance. The unique combination of mechanical properties makes the composite appealing for applications under various conditions, especially for absorbing mechanical energy and reducing vibrations and noise.

## 1. Introduction

Magnesium (Mg) and its alloys are promising among lightweight metals owing to their remarkably high specific (*i.e.*, normalized by density) strength and stiffness, good biocompatibility and unique biodegradability [1,2]. Mg alloys also demonstrate excellent damping properties which outperform those of most other metallic materials, and as such are appealing for reducing vibrations and noise [3,4]. However, the structural applications of Mg alloys are limited by their relatively low strengths at both ambient and elevated temperatures, especially when compared to widely used steels and aluminum alloys. Strengthening can be achieved in Mg alloy systems, by alloying, thermo-mechanical processing, or making Mg-based composites through the introduction of reinforcements [1,2,5–8]. Nevertheless, the resultant materials often display a clear decrease in their damping capacities,

especially when compared to pure Mg [9–11]. This is caused by the fact that the strength and damping capacity of metals originate principally from two contradictory strategies, respectively that of the obstruction and promotion of dislocation motion [9–13].

This conflict has been effectively overcome in our recent study by developing a Mg-based interpenetrating-phase composite reinforced with a 3-D printed Nitinol (NiTi) scaffold [14]. The bi-continuous nature of constituent phases allows for an effective stress transfer within them, thereby promoting a potent strengthening effect by the Nitinol while maintaining the good damping properties of pure Mg. The damping capacity of the composite can be additionally enhanced by the easy occurrence of local deformation and damage at the weak interfaces between the two phases. A stable stress plateau can also be achieved in the composite under compression owing to the confinement of local damages within each phase, thereby leading to a high energy absorption

\* Corresponding author. Shi-Changxu Innovation Center for Advanced Materials, Institute of Metal Research, Chinese Academy of Sciences, Shenyang, 110016, China.

\*\* Corresponding author.

E-mail addresses: [zengqianliu@imr.ac.cn](mailto:zengqianliu@imr.ac.cn) (Z. Liu), [mfqwang@cmu.edu.cn](mailto:mfqwang@cmu.edu.cn) (Q. Wang).

<https://doi.org/10.1016/j.compositesb.2021.108783>

Received 5 January 2021; Received in revised form 26 February 2021; Accepted 8 March 2021

Available online 11 March 2021

1359-8368/© 2021 Elsevier Ltd. All rights reserved.

efficiency. Moreover, the composite after deformation can recover its initial shape and strength to a large extent, simply through heat treatment. This is attributed to the shape memory effect caused by the martensite-to-austenite phase transformation in the Nitinol which compensates for the low creep resistance of the Mg matrix [15,16]. Such characteristic makes it possible to repeatedly absorb a large amount of mechanical energy which is highly desirable for resisting impact and reducing vibrations.

Potential industrial applications of the Mg–NiTi interpenetrating-phase composite are clearly apparent in automobiles, where the multiple sources of vibrations can lead to high strain rates exceeding  $1 \text{ s}^{-1}$ , with the temperature ranging from  $\sim 175 \text{ }^\circ\text{C}$ , e.g., in transmission cases, to over  $300 \text{ }^\circ\text{C}$  in engine pistons [6]. Our previous study revealed that the damping capacity of the composite can be continuously enhanced with increasing temperature [14]. To provide a basis for safety-critical design, it is of importance to clarify any effects of strain rate and temperature on the mechanical properties, especially the strength, energy absorption efficiency, and damage mechanisms. Moreover, as the composite is intended for use in applications involving energy absorption and vibration reduction, the compressive loading state was taken as the central concern of the current study.

## 2. Materials and methods

### 2.1. Composite fabrication

The Mg–NiTi interpenetrating-phase composite was fabricated into a cubic shape of dimensions of  $10 \times 10 \times 10 \text{ mm}^3$ , using a two-step procedure involving the 3-D printing of a Nitinol scaffold via selective laser melting and subsequent pressureless infiltration of a Mg melt into the scaffold [14]. In particular, the Nitinol scaffold was printed in the form of rhombic dodecahedrons, which represents a common architecture in natural materials [17,18]. The Mg and Nitinol phases are bi-continuous and interpenetrated in 3-D space in the composite such that each phase will retain integrity after removal of the other one. A small amount of  $\text{Mg}_2\text{Ni}$  precipitates and Ti-rich phase are formed, respectively, at the grain boundaries within the Mg matrix and near the interfaces between the Mg and Nitinol phases [14]. This is caused by the diffusion of nickel near the surfaces of the Nitinol scaffold into the Mg matrix. Full details about the fabrication and microstructure of the composite can be found in Ref. [14].

### 2.2. Characterization

Cubic samples were ground and polished to dimensions of  $\sim 9 \times 9 \times 9 \text{ mm}^3$ . Uniaxial compression tests were performed on these samples at ambient room temperature and elevated temperatures of  $200 \text{ }^\circ\text{C}$  and  $350 \text{ }^\circ\text{C}$  using an Instron 5982 testing system (Instron Corp., USA) equipped with an incubator to achieve constant temperatures. The samples were placed in the incubator for 20 min prior to mechanical testing for tests at elevated temperatures. The compression testing was carried out under displacement control with the strain rates fixed at  $10^{-3} \text{ s}^{-1}$ ,  $10^{-2} \text{ s}^{-1}$ ,  $10^{-1} \text{ s}^{-1}$  and  $1 \text{ s}^{-1}$  at each temperature. For comparison, samples of the constituent phase, with the same dimensions were also tested under the same conditions, specifically pure Mg solidified from the infiltration temperature and the 3-D printed Nitinol scaffold (with no Mg infiltration). At least three tests were repeated for each combination of strain rate and temperature. Results are presented in form of mean  $\pm$  standard deviation.

To explore the nature of the damage mechanisms, a set of samples was compressed at different strain rates and temperatures to a constant strain of 15% before unloading. Their surface morphologies were then examined using an Inspect F50 field-emission scanning electron microscope (SEM) (FEI, USA) operating at an accelerating voltage of 20 kV.

## 3. Results

### 3.1. Compressive properties: effects of strain rate and temperature

Figs. 1–3 show the compressive engineering stress-strain curves for the Mg–NiTi interpenetrating-phase composite along with those for pure Mg and the Nitinol scaffold at different strain rates and temperatures. Rule-of-mixtures approximations by simply treating the composite as the sum of Mg and Nitinol scaffold are also presented for comparison, as indicated by the dash curves. To be specific, the stress at a given strain in the composite,  $\sigma_{ROM}$ , was approximated by summing that of pure Mg,  $\sigma_{Mg}$ , weighted by its volume fraction,  $V_{Mg}$ , onto the stress in the Nitinol scaffold at the identical strain,  $\sigma_{NITi}$ , following the relationship  $\sigma_{ROM} = \sigma_{Mg}V_{Mg} + \sigma_{NITi}$ , where the volume fraction of Mg matrix in the composite was measured to be 64.1% [14]. It is seen that the composite invariably displays a stable stress plateau up to a strain of over 40% at all strain rates and temperatures, both after yielding and before the later steep increase in stress. Such behavior is common in porous materials and often suggests a high potency for energy absorption [18–22]. The stresses in the composite exceed those in the constituents over the majority of the strain range. It is noted here that the low Young's modulus of the composite at room temperature may be related to the weak interfaces between Mg and Nitinol phases which tend to cause easy sliding as reported for Mg–Fe composite [23–27]. The weak grain boundaries in the Mg matrix, due to the presence of  $\text{Mg}_2\text{Ni}$  precipitates [14], may also play a role in lowering the modulus. In comparison, the stress plateau can be obtained in pure Mg only at room temperature. The stress tends to exhibit a continuous increase with strain at elevated temperatures. Such a stress response is unfavorable for energy absorption applications where the applied stress generally remains stable during material deformation [5–8,15,20,21]. Additionally, the energy absorption efficiency of the Nitinol scaffold at room temperature can be degraded because of the obvious stress drop after reaching the peak stress. This appears to be caused by the buckling deformation or collapse of struts in the scaffold [14,18–22]. Such stress drop becomes far less evident at higher temperatures, implying an improved mechanical stability of the scaffold.

The maximum transmitted stress,  $\sigma_{tr}$ , and energy absorption efficiency,  $E_a$ , are two key parameters for evaluating the energy absorption performance of materials. In case of the presence of a stable stress plateau,  $\sigma_{tr}$  and  $E_a$  are defined respectively as the peak stress at the plateau stage and the area under stress-strain curve before the stress rises to the level of  $\sigma_{tr}$  again [14,22], as illustrated in Fig. 1a. Alternatively, for materials where the stress continuously increases with strain, e.g., for pure Mg at elevated temperatures,  $\sigma_{tr}$  can be determined according to the intersection between tangents of the near linear sections before and after the steep stress increase [20,21], as illustrated in Fig. 3a.  $E_a$  can then be quantified by the area under the stress-strain curve up to the strain corresponding to  $\sigma_{tr}$ .

Fig. 4 presents the variations of  $\sigma_{tr}$  and  $E_a$  as a function of strain rate at different temperatures for the Mg–NiTi composite as compared to pure Mg and the Nitinol scaffold. At given temperatures,  $\sigma_{tr}$  tends to increase monotonically with increasing strain rate in the composite and pure Mg. Such dependence can be described according to the empirical relationship in form of  $\sigma_{tr} = K\dot{\epsilon}^m$ , where  $\dot{\epsilon}$  is the strain rate and  $K$  and  $m$  are material constants which are temperature dependent [21,28–30]. At room temperature, the composite displays a markedly lower value of  $m$  (0.019) than those of bone (0.044–0.058) and dealloying-based metal-polymer composites (0.037–0.044) [31], implying a lower sensitivity of compressive properties to strain rate. With increase in temperature, the parameter  $m$  displays an increasing trend for the composite, indicating an improvement of the strain rate sensitivity. With respect to the energy absorption, the value of  $E_a$  exhibits a general increasing trend with increase in strain rate at all temperatures for both the composite and pure Mg. The values of  $\sigma_{tr}$  and  $E_a$  for the two materials are decreased

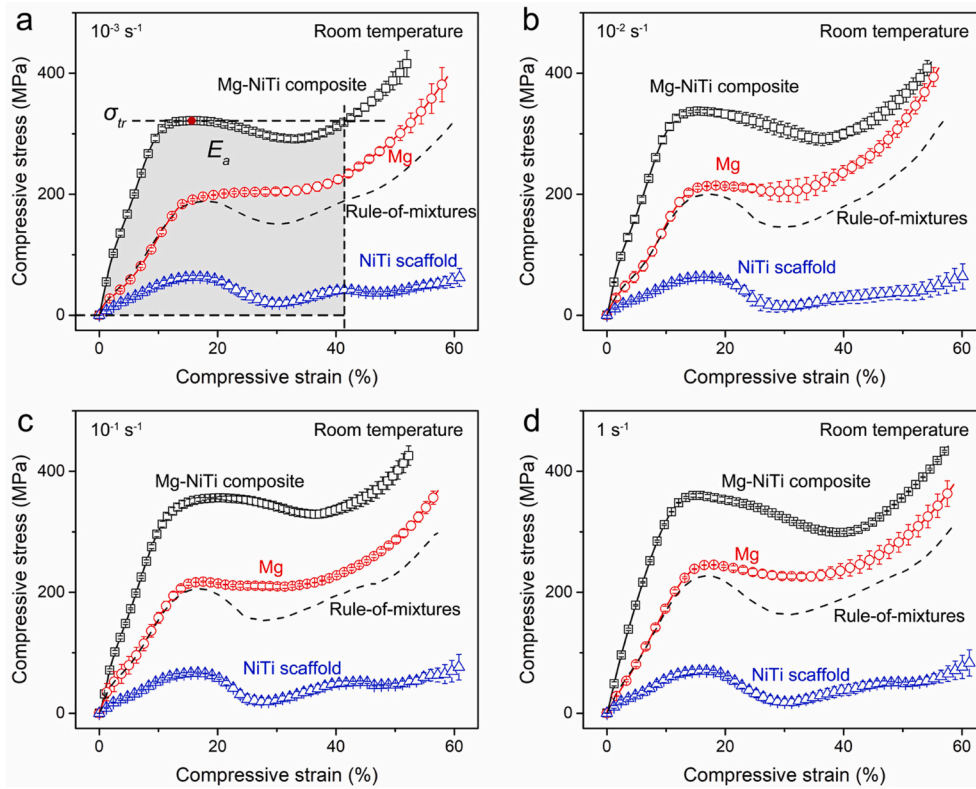


**Fig. 1.** Compressive engineering stress-strain curves of the Mg-NiTi interpenetrating-phase composite at varying strain rates at room temperature. The results for pure Mg, the Nitinol scaffold, and their combination according to the rule-of-mixtures are also shown for comparison. The stresses on each curve are presented in form of mean  $\pm$  standard deviation from those at equal strains for at least three samples. The maximum transmitted stress,  $\sigma_{tr}$ , and energy absorption efficiency,  $E_a$ , of the materials are indicated in (a) for the presence of a stable stress plateau [14,22].

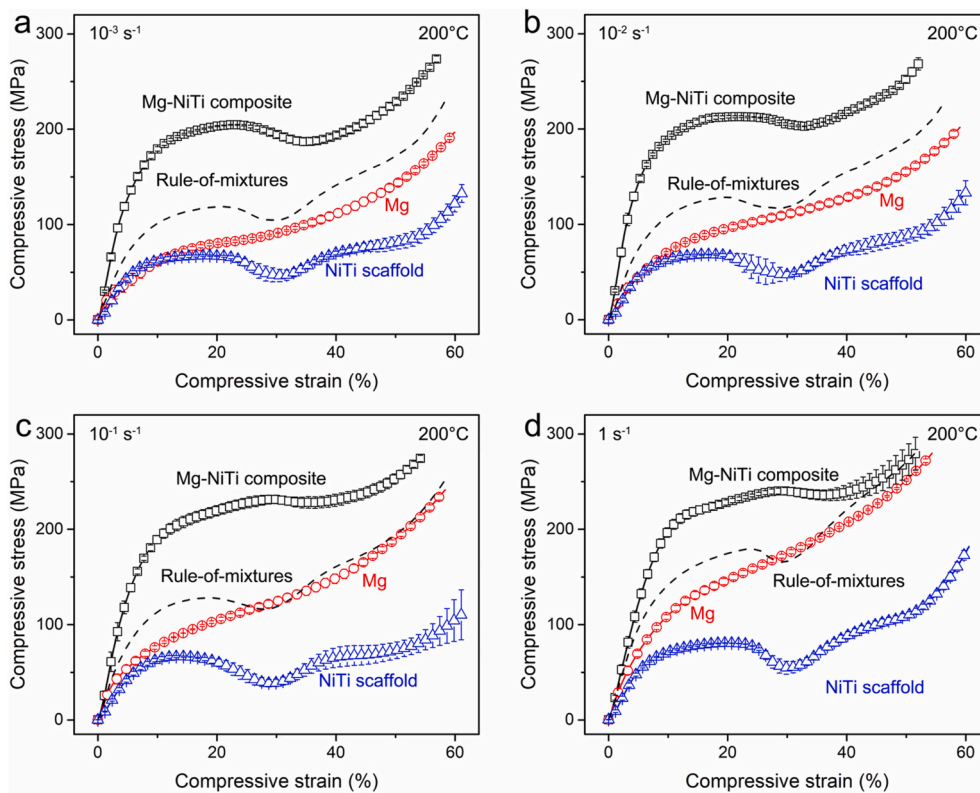


**Fig. 2.** Compressive engineering stress-strain curves of the Mg-NiTi interpenetrating-phase composite at varying strain rates at 200 °C as compared to pure Mg, the Nitinol scaffold, and their combination according to the rule-of-mixtures.

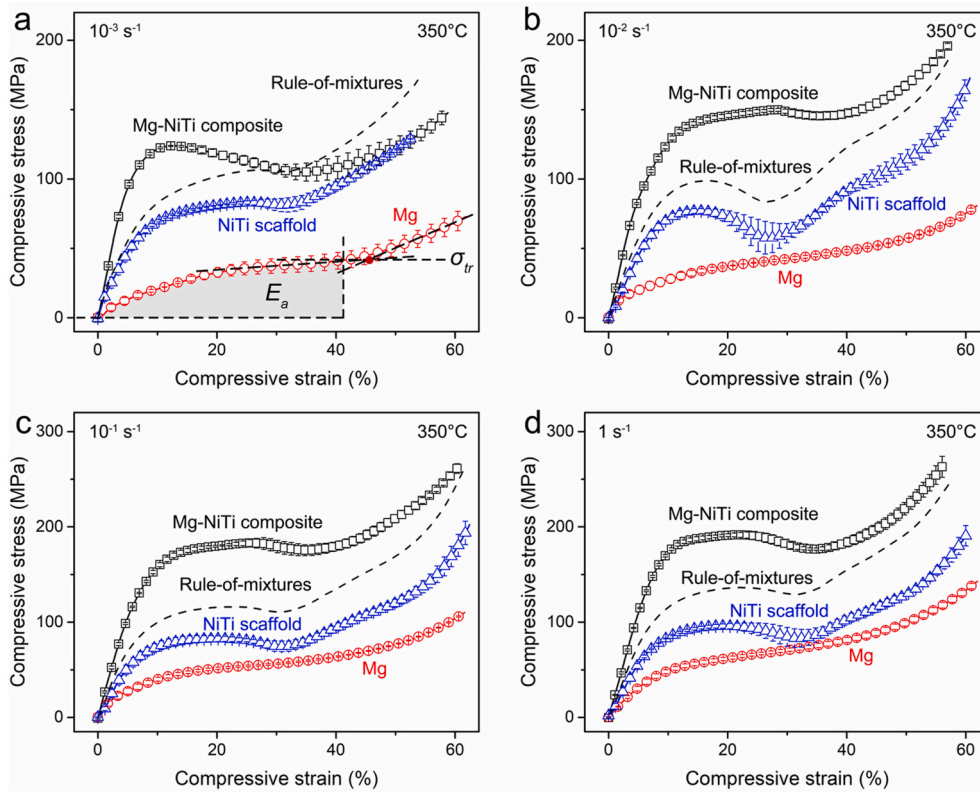


**Fig. 3.** Compressive engineering stress-strain curves at varying strain rates at 350 °C for the Mg–NiTi interpenetrating-phase composite and its constituents of pure Mg and the Nitinol scaffold along with their combination according to the rule-of-mixtures. Values of  $\sigma_{tr}$  and  $E_a$ , for materials where the stress continuously increases with strain, are indicated in (a) [20,21].

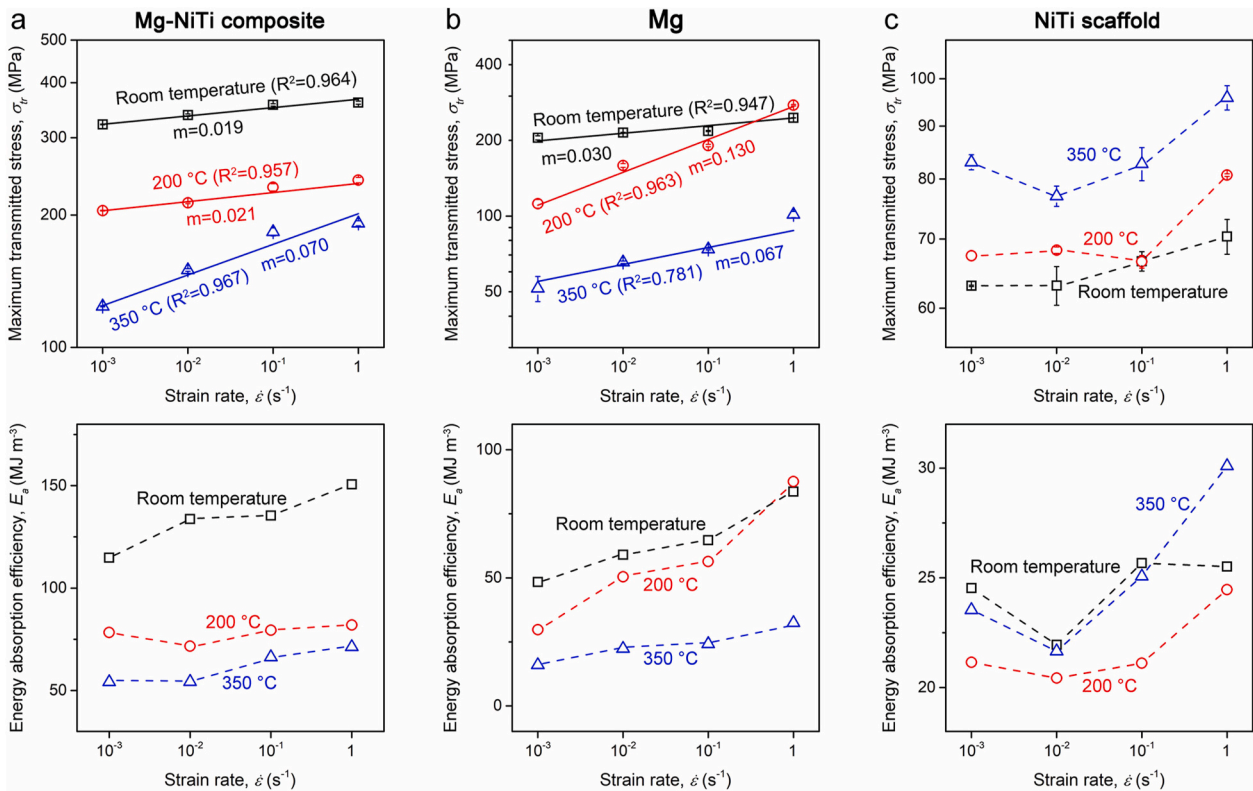


**Fig. 4.** Variation of the maximum transmitted stress,  $\sigma_{tr}$ , and energy absorption efficiency,  $E_a$ , as a function of strain rate,  $\dot{\epsilon}$ , at varying temperatures for (a) the Mg–NiTi interpenetrating-phase composite and its constituents of (b) pure Mg and (c) the Nitinol scaffold. The fitting results for the parameter  $m$  according to  $\sigma_{tr} = K\dot{\epsilon}^m$  for the Mg–NiTi composite and pure Mg are presented in (a) and (b).

as the temperature rises. Significantly, the composite is capable of absorbing a large amount of mechanical energy with  $E_a$  exceeding  $100 \text{ MJ m}^{-3}$  at all the strain rates tested at room temperature.

In contrast, the Nitinol scaffold displays an increasing maximum transmitted stress  $\sigma_{tr}$  with increase in temperature, yet does not show a clear temperature dependence for  $E_a$ . Such variations are considered to be associated with the unique phase constituents and deformation mechanisms of Nitinol which would likely be quite different depending on the specific strain rate and temperature. The characteristic start and finish temperatures for the austenite-to-martensite phase transformation during cooling,  $M_s$  and  $M_f$ , in the present Nitinol were  $\sim 64 \text{ }^\circ\text{C}$  and  $\sim 14 \text{ }^\circ\text{C}$ , respectively, as shown in Fig. S1 in the Supplementary Materials. The start and finish temperatures for the reverse transformation during heating,  $A_s$  and  $A_f$ , are  $\sim 56 \text{ }^\circ\text{C}$  and  $\sim 92 \text{ }^\circ\text{C}$ , respectively. As such, the Nitinol scaffold comprises martensite and remaining austenite phases at room temperature, but is composed almost entirely of austenite phase at elevated temperatures of  $200 \text{ }^\circ\text{C}$  and  $350 \text{ }^\circ\text{C}$ . In addition to the plastic deformation in the individual phases, the applied stress may even induce austenite-to-martensite phase transformation in the scaffold which would also be dependent on strain rate and temperature [16,32,33]. Therefore, the combined effects of strain rate and temperature may cause variations in a mixture of distinctly different deformation mechanisms in Nitinol, e.g., dislocation slip in the austenite and martensite phases, stress-induced austenite-to-martensite phase transformation, and twinning in the martensite phase [16,32–38], thereby leading to varying mechanical properties.

### 3.2. Constitutive analysis: strain rate and temperature sensitivities

The compressive true stress-strain curves of the three materials, shown in Fig. S2–S4, are analyzed below to quantitatively elucidate the

strain rate and temperature sensitivities of their mechanical properties. Specifically, the flow behavior of metallic materials at strain rate  $\dot{\epsilon}$  and absolute temperature  $T$  can be described according to the hyperbolic sine-type Arrhenius relationship following [21,39–42]:

$$\dot{\epsilon} = A [\sinh(\alpha\sigma_f)]^n \exp(-Q/RT) = Z \exp(-Q/RT) \quad (1)$$

where  $\sigma_f$  is the flow stress,  $R$  is the universal gas constant, and  $A$  and  $\alpha$  are material constants. The stress exponent,  $n$ , and apparent activation energy,  $Q$ , are two key parameters depicting the effects of strain rate and temperature with their values negatively correlated, respectively, with the strain rate and temperature sensitivities of the flow stress [39–42]. The Zener-Holloman parameter  $Z$ , with  $Z = A[\sinh(\alpha\sigma_f)]^n = \dot{\epsilon} \exp(Q/RT)$ , is introduced for mathematical simplification in determining  $n$  [41,42]. To quantify the parameter  $\alpha$ , Eq. (1) can be approximated, respectively, using an exponential relationship at relatively high stress level and a power law relationship at relatively low stress level as [40,41]:

$$\dot{\epsilon} = \begin{cases} A_h \exp(\gamma\sigma_f) \exp(-Q/RT) & (\text{high stress level}) \\ A_l \sigma_f^\beta \exp(-Q/RT) & (\text{low stress level}) \end{cases} \quad (2)$$

where  $A_h$  and  $A_l$  are material constants, akin to  $A$ , corresponding respectively to high and low stress levels.  $\alpha$  can be determined as  $\alpha = \gamma/\beta$  from the newly introduced parameters  $\gamma$  and  $\beta$  which can be readily obtained by data fitting.

As shown in Fig. 5a and b, the peak flow stress  $\sigma_p$ , i.e., the maximum value of flow stress on the true stress-strain curves before final steep stress increase (Fig. S2–S4), for the composite and its constituents at relatively high and low stress levels can be well described according to Eq. (2). It is noted here that, for the composite and pure Mg, the high and low stress levels correspond to testing temperatures of room

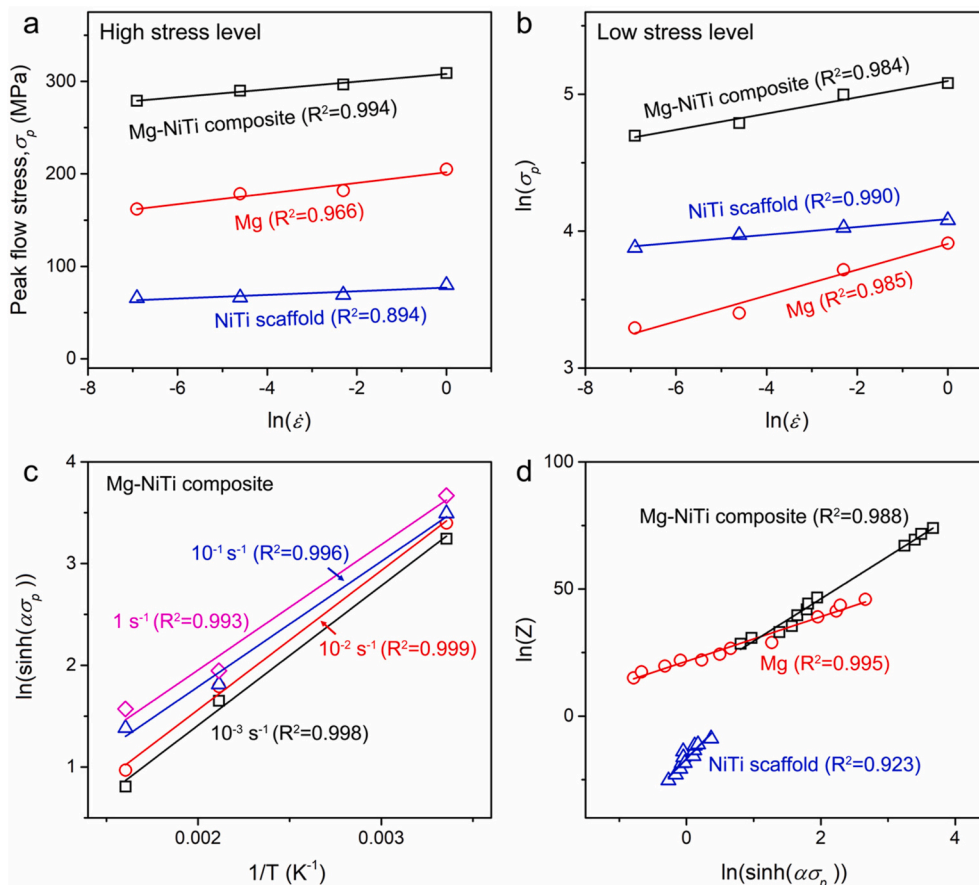


**Fig. 5.** Fitting results for the flow behavior of the Mg–NiTi interpenetrating-phase composite as compared to pure Mg and the Nitinol scaffold. (a, b) Relationships between the peak flow stress  $\sigma_p$  and strain rate  $\dot{\epsilon}$  for the three materials at their relatively (a) high and (b) low stress levels. (c) Fitting of  $\ln[\sinh(\alpha\sigma_p)]-1/T$  relationships at different strain rates for the Mg–NiTi composite in determining the apparent activation energy  $Q$ . The results for pure Mg and the Nitinol scaffold are shown in Figure S5. (d) Fitting of  $\ln Z-\ln[\sinh(\alpha\sigma_p)]$  relationships for the three materials in determining the stress exponent  $n$ .

temperature and 350 °C, respectively, in view of the decreasing trend of their flow stress with rising temperature. Nevertheless, the test temperature of 350 °C and room temperature are considered for the high and low stress levels for the Nitinol scaffold because of its opposite dependence of flow stress on temperature.

The parameters  $\gamma$  and  $\beta$  can be determined, respectively, as the reciprocals of slopes for  $\sigma_p$ - $\ln\dot{\epsilon}$  at high stress level and  $\ln\sigma_p$ - $\ln\dot{\epsilon}$  at low stress level, giving the values of  $\alpha$ . Additionally, the apparent activation energy,  $Q$ , can be obtained by differentiating the logarithmic form of Eq. (1) as:

$$Q = R \left[ \frac{\partial \ln \dot{\epsilon}}{\partial \ln [\sinh(\alpha \sigma_p)]} \right]_T \left[ \frac{\partial \ln [\sinh(\alpha \sigma_p)]}{\partial (1/T)} \right]_i \quad (3)$$

For each material, the value of  $\partial \ln [\sinh(\alpha \sigma_p)] / \partial (1/T)$  can be determined as the average of the slopes of fitting lines for  $\ln [\sinh(\alpha \sigma_p)] - 1/T$ , which are nearly the same at different strain rates, as shown in Fig. 5c and S5. The value of  $\partial \ln \dot{\epsilon} / \partial \ln [\sinh(\alpha \sigma_p)]$  can be determined as the average reciprocal of the slopes of fitting lines for  $\ln [\sinh(\alpha \sigma_p)] - \ln \dot{\epsilon}$  at different temperatures, as shown in Fig. S6. By incorporating  $Q$ , the parameter  $Z$  for different strain rates and temperatures can be obtained from  $Z = \dot{\epsilon} \exp(Q/RT)$ . As such, the parameters  $A$  and  $n$  can be determined using the intercept and slope of the fitting lines for  $\ln Z - \ln [\sinh(\alpha \sigma_p)]$  according to Eq. (1), as shown in Fig. 5d. The fitting results for all these parameters are listed in Table S1 in the Supplementary Materials. The values of these parameters for pure Mg conform well to those reported in literature [39,41], indicating a good validity of the above analysis.

As shown in Fig. 6a–c, the general varying trends of peak flow stress with strain rate and temperature can be well expressed by Eq. (1) for all the three materials, despite the fact that the relatively lower goodness-of-fit for the Nitinol scaffold can be associated with the changes in the deformation mechanisms discussed above. Fig. 6d presents a direct comparison of the strain rate and temperature sensitivities of the peak flow stress for the three materials, which are negatively correlated with

the stress exponent  $n$  and apparent activation energy  $Q$ , respectively. It is seen that the Mg–NiTi interpenetrating-phase composite displays the largest  $Q$ , implying the lowest temperature sensitivity of the flow stress. Also, the parameter  $n$  of the composite exceeds that of pure Mg by ~90%. These results suggest a markedly enhanced stability of the compressive properties in the composite with respect to strain rate and temperature as compared to the Mg matrix. This clearly is achieved through the introduction of the continuous Nitinol scaffold reinforcement.

### 3.3. Damage mechanisms

Our previous study has revealed that the damage processes in the Mg–NiTi interpenetrating-phase composite under quasi-static compression at a strain rate of  $10^{-3} \text{ s}^{-1}$ , originates at room temperature principally from the grain boundary cracking of the Mg matrix near the  $\text{Mg}_2\text{Ni}$  precipitates [14]. As the damage evolves, this is followed by the interfacial separation between the Mg and Nitinol and the cracking (to destruction) of the Nitinol scaffold with the increase in compressive strain [14]. Here the morphology of damage in the composite was further examined to discern the effects of strain rate and temperature on the dominant damage mechanisms. In view of the potential applications for energy absorption, all the samples for this particular characterization were pre-compressed to a fixed strain of 15% which approximately corresponds to the onset of stress plateau on stress-strain curves.

Fig. 7 shows representative surface morphologies of the composite after compression at different strain rates and temperatures; these demonstrate a distinct dependence of damage mechanisms on the strain rate and temperature. At a low strain rate of  $10^{-3} \text{ s}^{-1}$ , grain boundary cracking of the Mg matrix is consistently the prime damage mechanism at varying temperatures. This is largely associated with the presence of  $\text{Mg}_2\text{Ni}$  precipitates at the grain boundaries [14]. With increase in strain rate, interfacial cracking between Mg and Nitinol plays an increasing

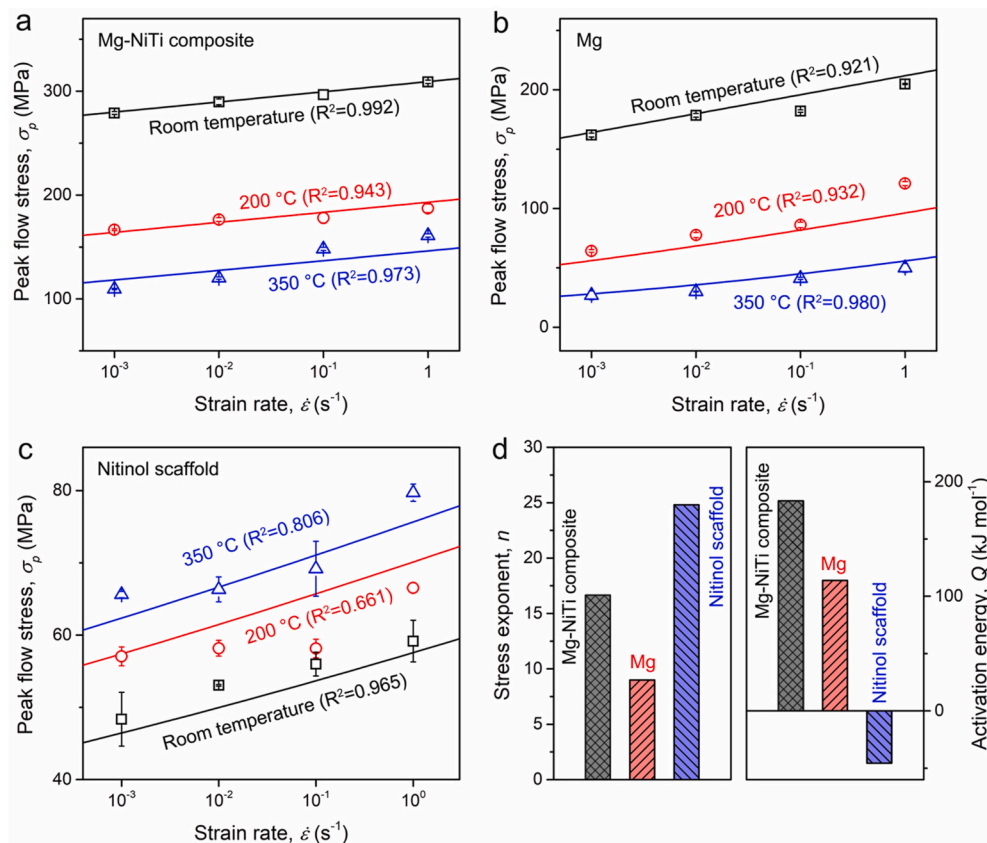


**Fig. 6.** Theoretical description about the peak flow stress and its sensitivities to strain rate and temperature. Dependences of peak flow stress on strain rate at varying temperatures for (a) the Mg–NiTi interpenetrating-phase composite, (b) pure Mg, and (c) the Nitinol scaffold described by the theoretical model according to Eq. (1). (d) Comparison of the strain rate and temperature sensitivities of the peak flow stress for the three materials in terms of stress exponent  $n$  and apparent activation energy  $Q$ .

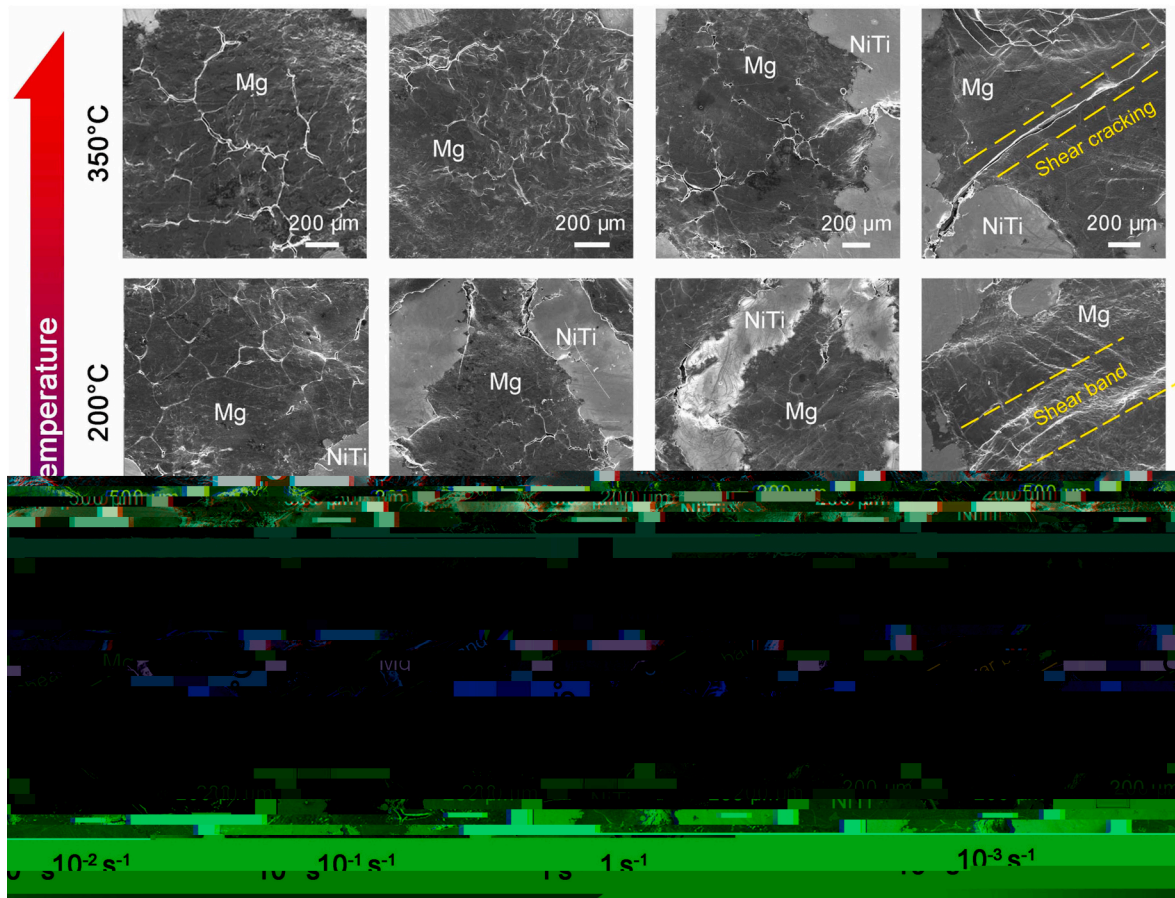


Fig. 7. Representative damage morphologies of the Mg–NiTi composite after compression at different strain rates and temperatures. All the samples were compressed to a fixed strain of 15%, which corresponds to the onset of the stress plateau, and then unloaded for characterization.

role in causing damage at room temperature up to 200 °C. This suggests an enhanced incompatibility of deformation between the two phases which can be likely ascribed to the micro-inertia in heterogeneous materials at dynamic loading conditions [43–45]. The precipitation of a Ti-rich phase at the interfaces also plays a role in promoting the interfacial cracking [14]. Specifically, both grain boundary cracking and interfacial cracking occur in the composite at 200 °C at strain rates of  $10^{-2} \text{ s}^{-1}$  and  $10^{-1} \text{ s}^{-1}$ . The coexistence of the two modes implies a gradual transition of the damage mechanisms with varying strain rate and temperature.

The damage in the composite at 350 °C and for strain rates below  $1 \text{ s}^{-1}$  is still governed by the grain boundary cracking in the Mg matrix. Nevertheless, the detailed characteristics of the cracking of the grain boundaries are largely dependent on temperature. The cracks are primarily localized at a limited number of grain boundaries at room temperature; however, they are more uniformly distributed as the temperature increases. This is consistent with the general trend in metals that grain boundaries tend to become less resistant to fracture at elevated temperatures [15,39,41]. With the further increase of strain rate up to  $1 \text{ s}^{-1}$  at temperatures of 200 °C and 350 °C, the composite displays a dominant damage mode of shear cracking, which is likely caused by the localized heat accumulation generated from the instantaneous plastic deformation [46–49]. In this case, the global fracture of the composite necessitates the penetration of shear bands and cracks through both the Mg and Nitinol phases. However, owing to their interpenetrating-phase architecture in 3-D space, the propagation of shear bands and cracks can be effectively arrested at the Nitinol scaffold, especially at room temperature. This crack arresting feature is highly favorable for absorbing mechanical energy in the composite under

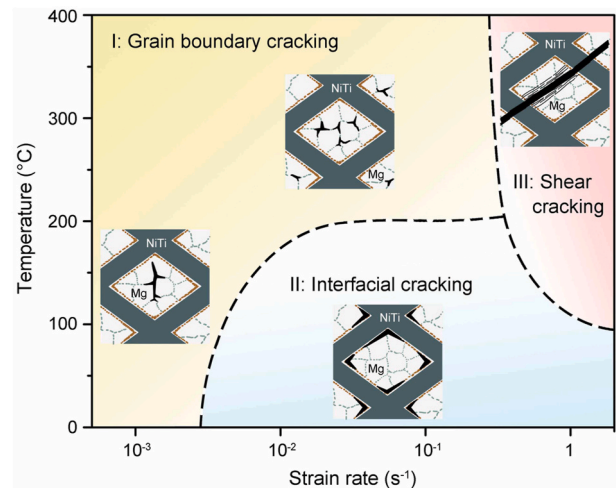


Fig. 8. Dominant damage mechanisms in the Mg–NiTi interpenetrating-phase composite as a function of strain rate and temperature. The damage mechanisms were categorized into three regions representing grain boundary cracking of the Mg matrix, interfacial cracking between Mg and Nitinol phases and shear cracking. The insets show the schematic illustrations of corresponding mechanisms.

dynamic loading. Therefore, the damage mechanisms of the composite can be categorized into three typical regions as a function of the strain rate and temperature, as illustrated in Fig. 8. It is noted here that there are gradual transitions or a mixture of mechanisms, instead of sharp changes, between adjacent regions at their boundaries as indicated by the dashed curves.

#### 4. Discussion

The above results clearly demonstrate a large dependency of the compressive properties of the Mg–NiTi interpenetrating-phase composite on strain rate and temperature which are markedly different from those for pure Mg and the Nitinol scaffold. Such characteristics are significant for potential applications of this composite, e.g., for absorbing mechanical energy or reducing vibrations and noise, where varying strain rates and temperatures are frequently involved. The unique feature of this composite stems essentially from the combination of its two constituents and their 3-D interpenetrating-phase architecture. On the one hand, in contrast to the easy creep and obvious weakening of pure Mg at elevated temperatures, the compressive properties of the composite are remarkably less sensitive to temperature at different strain rates, as inferred by the much higher value of the apparent activation energy  $Q$  (Fig. 6d). This is largely associated with the low temperature sensitivity of the properties in the Nitinol phase which can even be improved with increasing temperature (Fig. 4b). As such, the Nitinol scaffold within the composite plays an increasing role in carrying load and absorbing mechanical energy with increase in temperature. The stress transfer within the Nitinol scaffold and the Mg matrix, and that between them, can be facilitated, respectively, by the bi-continuous nature of the two phases and their 3-D interpenetrating-phase architecture. This helps promote an effective reinforcing role of the Nitinol scaffold in the composite. Such a feature differs markedly from the case for composites containing discrete reinforcements where the strengthening effect of reinforcements can be notably degraded when the matrix becomes weakened [5–8,12].

On the other hand, the Mg–NiTi composite constantly exhibits a stable compressive stress plateau at different strain rates and temperatures, which is favorable for energy absorption under various conditions. The 3-D interpenetrating-phase architecture plays a critical role in enhancing the damage tolerance of the composite, thereby generating the stable stress plateau for effective energy absorption. First, mechanical damages, especially at the early stages, can be confined to each individual constituent of the Mg and Nitinol owing to their interpenetration and mutual partition in 3-D space. This helps retard the occurrence of outright failure in the entire composite caused by critical propagation of damage across the two phases. Specifically, the propagation of grain boundary cracks out of the Mg matrix inevitably encounters the barriers induced by the Nitinol scaffold, as shown in Fig. S7. Second, the continuous nature of the Nitinol scaffold can effectively mitigate the weakening effects caused by grain boundary cracking and creep of the Mg matrix. Additionally, interfacial cracking between the Mg and Nitinol phases cannot lead to a complete separation of them because they are interpenetrated and geometrically interlocked. The composite can thus retain its structural integrity even when the interfacial cracks penetrate into the Nitinol scaffold [14]. Moreover, the 3-D interpenetrating-phase architecture also functions to resist global fracture of the composite under dynamic loading conditions as it necessitates the propagation of shear bands and cracks through the Nitinol scaffold (Fig. S7). The contact and further compaction between adjacent struts of the Nitinol scaffold after it ruptures lead to the increase of stress with strain, thereby causing the termination of the stress plateau.

Fig. 9 shows a direct comparison of the compressive properties, in terms of the maximum transmitted stress  $\sigma_{tr}$  and the energy absorption efficiency  $E_a$ , for the current Mg–NiTi composite, pure Mg and the Nitinol scaffold at different strain rates and temperatures. Typical property ranges of other metallic materials at room temperature are also

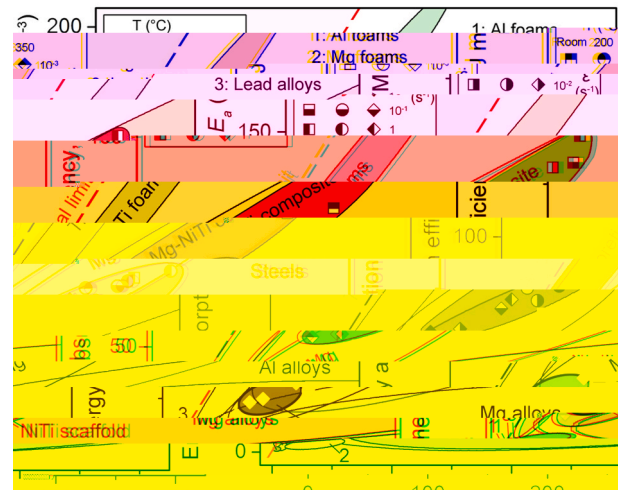


Fig. 9. Comparison of the maximum transmitted stress  $\sigma_{tr}$  and energy absorption efficiency  $E_a$  under compression for the Mg–NiTi interpenetrating-phase composite with those of other typical metallic materials [7,8,14–22,28,50]. The theoretical limit for energy absorption, which corresponds to the ideal case where the stress constantly equals  $\sigma_{tr}$  over the entire range of strain up to 100%, is indicated by the dashed line [22].

plotted to provide a clearer recognition [7,8,14–22,28,50]. The theoretical limit of  $E_a$ , as indicated by the dashed line, corresponds to the ideal case of energy absorption for materials where the stress constantly equals  $\sigma_{tr}$  at the entire range of strain up to 100% [22]. It is noted here that most Mg alloys are inferior to pure Mg in absorbing mechanical energy, despite their higher strengths, as they usually display marked strain-hardening behavior with continuously rising stress-strain curves, or they simply fail with less plastic deformation [19,21,50], in either case lacking a stress plateau. It can be seen that the Mg–NiTi composite outperforms its constituents in both  $\sigma_{tr}$  and  $E_a$  over the majority of tested strain rate and temperature ranges (except for the condition of  $1 \text{ s}^{-1}$  at  $200^\circ\text{C}$ ). In particular, the energy absorption efficiency of the composite is much closer to the theoretical limit as compared to most Mg and aluminum alloys. Its compressive properties, specifically the energy absorption efficiency, are even comparable to those of some steels, such as the Q235 low-carbon steel [19], which have far higher densities. Moreover, our previous study has revealed that the composite has outstanding damping capacities under varying strain amplitudes at room to elevated temperatures [14]. The excellent combination of these properties may help expand the potential use of this composite to a much broader range of applications, from quasi-static to dynamic loading conditions and from room to elevated temperatures, particularly for applications involving energy absorption and vibration/noise reduction.

#### 5. Conclusions

The compressive properties of our Mg–NiTi interpenetrating-phase composite, with special reference to their dependences on strain rate and temperature, are investigated here and compared to the corresponding properties of its constituents, that of pure Mg and Nitinol scaffold. Based on this study, the following conclusions can be drawn:

- (1) The composite demonstrates an effective energy absorption efficiency at varying strain rates and temperatures which is characterized by the presence of a stable stress plateau on the stress-strain curves up to large strains of more than 40%. The plateau stress exceeds those for the individual constituents as well as their combination according to the rule-of-mixtures.

- (2) The composite exhibits different compressive properties and various damage mechanisms depending on different strain rates and temperatures; these include grain boundary cracking of the Mg matrix, interfacial cracking between the Mg and Nitinol phases, and shear cracking. The maximum transmitted stress and energy absorption efficiency display a general increasing trend with increase in strain rate or decrease in temperature. The strain rate and temperature sensitivities of compressive properties are much lower in the composite as compared to pure Mg, indicating an enhanced stability for the composite.
- (3) The 3-D interpenetrating-phase architecture plays a central role in ensuring an effective strengthening effect of the Nitinol scaffold and resisting damage evolution in the composite, thereby endowing it with remarkable damage tolerance for potent energy absorption. The good combination of properties, *i.e.*, the maximum transmitted stress, energy absorption efficiency and damping capacities, makes the Mg–NiTi interpenetrating-phase composite appealing for applications under various conditions where different strain rates and temperatures may be involved, especially for energy absorption and vibration/noise reduction.

#### Data availability

The data that support the findings of this study are available from the corresponding author, Prof. Zengqian Liu, at [zengqianliu@imr.ac.cn](mailto:zengqianliu@imr.ac.cn), upon reasonable request.

#### CRedit authorship contribution statement

**Mingyang Zhang:** Methodology, Formal analysis, Investigation, Writing – original draft. **Qin Yu:** Formal analysis, Writing – review & editing. **Zengqian Liu:** Conceptualization, Writing – review & editing, Supervision. **Jian Zhang:** Methodology, Data curation. **Da Jiao:** Investigation, Project administration. **Shujun Li:** Investigation, Visualization. **Hui Peng:** Validation, Resources. **Qiang Wang:** Conceptualization, Formal analysis. **Zhefeng Zhang:** Resources, Funding acquisition. **Robert O. Ritchie:** Supervision.

#### Declaration of competing interest

The authors declare that they have no known competing financial interests or personal relationships that could have appeared to influence the work reported in this paper.

#### Acknowledgements

The authors are grateful for the financial support by the National Key R&D Program of China under grant number 2020YFA0710404, the National Natural Science Foundation of China under grant number 51871216, the KC Wong Education Foundation under grant number GJTD-2020-09, the LiaoNing Revitalization Talents Program, the State Key Laboratory for Modification of Chemical Fibers and Polymer Materials at Donghua University, the Opening Project of Jiangsu Province Key Laboratory of High-End Structural Materials under grant number hsm1801, the Opening Project of National Key Laboratory of Shock Wave and Detonation Physics under grant number 6142A03203002, and the Youth Innovation Promotion Association CAS. ROR was supported by the Multi-University Research Initiative under grant number AFOSR-FA9550-15-1-0009 from the Air Force Office of Scientific Research.

#### Appendix A. Supplementary data

Supplementary data to this article can be found online at <https://doi.org/10.1016/j.compositesb.2021.108783>.

#### References

- [1] Pollock TM. Weight loss with magnesium alloys. *Science* 2010;328:986–7.
- [2] Agnew SR. Wrought magnesium: a 21st century outlook. *JOM* 2004;56:20–1.
- [3] Watanabe H, Sawada T, Sasakura Y, Ikeo N, Mukai T. Microyielding and damping capacity in magnesium. *Scripta Mater* 2014;87:1–4.
- [4] Schaller R. Metal matrix composites, a smart choice for high damping materials. *J Alloys Compd* 2003;355:131–5.
- [5] Trang TTT, Zhang JH, Kim JH, Zargarani A, Hwang JH, Suh BC, Kim NJ. Designing a magnesium alloy with high strength and high formability. *Nat Commun* 2018;9:2522.
- [6] Luo AA. Recent magnesium alloy development for elevated temperature applications. *Int Mater Rev* 2004;49:13–30.
- [7] Ye HZ, Liu XY. Review of recent studies in magnesium matrix composites. *J Mater Sci* 2004;39:6153–71.
- [8] Tang S, Xin TZ, Xu WQ, Miskovic D, Sha G, Quadir Z, Ringer S, Nomoto K, Birbilis N, Ferry M. Precipitation strengthening in an ultralight magnesium alloy. *Nat Commun* 2019;10:1003.
- [9] Li QY, Li J, He G. Compressive properties and damping capacities of magnesium reinforced with continuous steel wire. *Mater Sci Eng, A* 2017;680:92–6.
- [10] Parande G, Manakari V, Koppa SDS, Gupta M. A study on the effect of low-cost eggshell reinforcement on the immersion, damping and mechanical properties of magnesium-zinc alloy. *Compos Part B* 2020;182:107650.
- [11] Gu JH, Zhang XN, Gu MY. Mechanical properties and damping capacity of (SiC<sub>p</sub> + Al<sub>2</sub>O<sub>3</sub>-SiO<sub>2</sub>)/Mg hybrid metal matrix composite. *J Alloys Compd* 2004;385:104–8.
- [12] Ritchie RO. The conflicts between strength and toughness. *Nat Mater* 2011;10:817–22.
- [13] Razzaghi M, Kasiri-Asgarani M, Bakhsheshi-Rad HR, Ghayour H. Microstructure, mechanical properties, and in-vitro biocompatibility of nano- NiTi reinforced Mg-3Zn-0.5Ag alloy: prepared by mechanical alloying for implant applications. *Compos Part B* 2020;190:107947.
- [14] Zhang MY, Yu Q, Liu ZQ, Zhang J, Tan GQ, Jiao D, Zhu WJ, Li SJ, Zhang ZF, Yang R, Ritchie RO. 3D printed Mg–NiTi interpenetrating-phase composites with high strength, damping capacity, and energy absorption efficiency. *Sci Adv* 2020;6:eaba5581.
- [15] Humbeeck JV. Damping capacity of thermoelastic martensite in shape memory alloys. *J Alloys Compd* 2003;355:58–64.
- [16] Milička K, Cadek J, Rys P. High temperature creep mechanisms in magnesium. *Acta Mater* 1970;18:1071–82.
- [17] Vyatskikh A, Delalande S, Kudo A, Zhang X, Portela CM, Greer JR. Additive manufacturing of 3D nano-architected metals. *Nat Commun* 2018;9:593.
- [18] Schaedler TA, Jacobsen AJ, Torrents A, Sorensen AE, Lian J, Greer JR, Valdevit L, Carter WB. Ultralight metallic microlattices. *Science* 2011;334:962–5.
- [19] Haghpanah B, Salari-Sharif L, Pourrajab P, Hopkins J, Valdevit L. Multistable shape-reconfigurable architected materials. *Adv Mater* 2016;28:7915–20.
- [20] Paul A, Ramamurty U. Strain rate sensitivity of a closed-cell aluminum foam. *Mater Sci Eng, A* 2000;281:1–7.
- [21] Yue XZ, Fukazawa H, Kitazono K. Strain rate sensitivity of open-cell titanium foam at elevated temperature. *Mater Sci Eng, A* 2016;673:83–9.
- [22] Schaedler TA, Ro CJ, Sorensen AS, Eckel Z, Yang SS, Carter WB, Jacobsen AJ. Designing metallic microlattices for energy absorber applications. *Adv Eng Mater* 2014;16:276–83.
- [23] Okulov IV, Wilmers J, Joo SH, Bargmann S, Kim HS, Kato H. Anomalous compliance of interpenetrating-phase composite of Ti and Mg synthesized by liquid metal dealloying. *Scripta Mater* 2021;194:113660.
- [24] Okulov IV, Geslin PA, Soldatov IV, Ovri H, Joo SH, Kato H. Anomalous low modulus of the interpenetrating-phase composite of Fe and Mg obtained by liquid metal dealloying. *Scripta Mater* 2019;163:133–6.
- [25] Pérez P, Garcés G, Adeva P. Mechanical properties of a Mg-10 (vol.%)Ti composite. *Compos Sci Technol* 2004;64:145–51.
- [26] Li DS, Zhang XP, Xiong ZP, Mai YM. Lightweight NiTi shape memory alloy based composites with high damping capacity and high strength. *J Alloys Compd* 2010;490:L15–9.
- [27] Yu C, Kang GZ, Fang DN. A micromechanical constitutive model for unusual temperature-dependent deformation of Mg-NiTi composites. *Int J Solid Struct* 2019;170:38–52.
- [28] Shen JH, Lu GX, Ruan D. Compressive behaviour of closed-cell aluminium foams at high strain rates. *Compos Part B* 2010;41:678–85.
- [29] Luo J, Li MQ, Yu WX, Li H. The variation of strain rate sensitivity exponent and strain hardening exponent in isothermal compression of Ti-6Al-4V alloy. *Mater Des* 2010;31:741–8.
- [30] Sassi S, Tarfaoui M, Nachtane M, Yahia HB. Strain rate effects on the dynamic compressive response and the failure behavior of polyester matrix. *Compos Part B* 2019;174:107040.
- [31] Okulov AV, Volegov AS, Weissmüller J, Markmann J, Okulov IV. Dealloying-based metal-polymer composites for biomedical applications. *Scripta Mater* 2018;146:290–4.
- [32] Iijima M, Ohno H, Kawashima I, Endo K, Mizoguchi I. Mechanical behavior at different temperatures and stresses for superelastic nickel–titanium orthodontic wires having different transformation temperatures. *Dent Mater* 2002;18:88–93.
- [33] Chen WN, Wu QP, Kang JH, Winfree NA. Compressive superelastic behavior of a NiTi shape memory alloy at strain rates of 0.001–750 s<sup>-1</sup>. *Int J Solid Struct* 2001;38:8989–98.
- [34] Gao YP, Zhang YF, Wang YZ. Determination of twinning path from broken symmetry: a revisit to deformation twinning in bcc metals. *Acta Mater* 2020;196:280–94.

- [35] Itin VI, Gyunter VE, Shabalovskaya SA, Sachdeva RLC. Mechanical properties and shape memory of porous Nitinol. *Mater Char* 1994;32:179–87.
- [36] Saigal A, Fonte M. Solid, shape recovered “bulk” Nitinol: part I-tension-compression asymmetry. *Mater Sci Eng, A* 2011;528:5536–50.
- [37] Cai S, Schaffer JE, Ren Y, Yu C. Texture evolution during nitinol martensite detwinning and phase transformation. *Appl Phys Lett* 2013;103:241909.
- [38] Ford DS, White SR. Thermomechanical behavior of 55Ni45Ti nitinol. *Acta Mater* 1996;44:2295–307.
- [39] Arun MS, Chakkingal U. A constitutive model to describe high temperature flow behavior of AZ31B magnesium alloy processed by equal-channel angular pressing. *Mater Sci Eng, A* 2019;754:659–73.
- [40] Wang JJ, Wen LH, Xiao JY, Liang TF, Hu XY, Li PH. The mechanical properties and constitutive model of two woven composites including the influences of temperature, strain rate and damage growth. *Compos Part B* 2019;161:502–13.
- [41] Li HY, Fan LL, Zhou MY, Zhou YL, Jiang K, Chen Y. Hot compression deformation and activation energy of nanohybrid-reinforced AZ80 magnesium matrix Composite. *Metals* 2020;10:119.
- [42] Chen L, Zhao GQ, Yu JQ. Hot deformation behavior and constitutive modeling of homogenized 6026 aluminum alloy. *Mater Des* 2015;74:25–35.
- [43] Wang Z, Poh LH. A homogenized localizing gradient damage model with micro inertia effect. *J Mech Phys Solid* 2018;116:370–90.
- [44] Gavriljuk S, Saurel R. Mathematical and numerical modeling of two-phase compressible flows with micro-inertia. *J Comput Phys* 2002;175:326–60.
- [45] Wang ZP, Sun CT. Modeling micro-inertia in heterogeneous materials under dynamic loading. *Wave Motion* 2002;36:473–85.
- [46] Chino Y, Kobata M, Iwasaki H, Mabuchi M. An investigation of compressive deformation behaviour for AZ91 Mg alloy containing a small volume of liquid. *Acta Mater* 2003;51:3309–18.
- [47] Jiang LH, Yang Y, Wang Z, Hu HB. Microstructure evolution within adiabatic shear band in peak aged ZK60 magnesium alloy. *Mater Sci Eng, A* 2018;711:317–24.
- [48] Fatemi-Varzaneh SM, Zarei-Hanzaki A, Cabrera JM. Shear banding phenomenon during severe plastic deformation of an AZ31 magnesium alloy. *J Alloys Compd* 2011;509:3806–10.
- [49] Yang Y, Yang SJ, Jiang LH. Study on the microstructural characteristics of adiabatic shear band in solid-solution treated ZK60 magnesium alloy. *Mater Char* 2019;156:109840.
- [50] Ashby MF. In: *Materials selection in mechanical design*, vol. 3. Oxford: Pergamon Press; 2005.